RSC Advances

PAPER

View Article Online
View Journal | View Issue

Cite this: *RSC Adv.*, 2016, **6**, 71070

Efficient perovskite light-emitting diodes by film annealing temperature control†

Junqing Liang,[ab] Yongqiang Zhang,[ab] Xiaoyang Guo,*[a] Zhihong Gan,[a] Jie Lin,[a] Yi Fan[a] and Xingyuan Liu*[a]

Received 3rd June 2016
Accepted 18th July 2016

DOI: 10.1039/c6ra14393h

www.rsc.org/advances

Perovskite light-emitting diodes (PeLEDs) have attracted much attention in the past two years due to their high photo-luminescence quantum efficiencies and wavelength tuneable characteristics. In this work, the effect of annealing temperature and time on the perovskite ($CH_3NH_3PbBr_3$) films and devices have been investigated in detail. The properties including photoluminescence, crystallinity and morphology of perovskite films together with device performance have been affected significantly by the annealing temperature and time. The PeLED with 80 °C annealing for 20 min shows the best device performance and exhibits a maximum luminance of 13 700 cd m^{-2}, and a maximum current efficiency of 8.22 cd A^{-1}. This work will provide useful information for the future optimization and development in high quality perovskite films and high performance PeLEDs.

Introduction

Organic–inorganic lead halide perovskite materials have attracted great research interest for perovskite solar cells due to their high power conversion of over 20%.[1,2] Very recently, perovskite light-emitting diodes (PeLEDs) have been reported and have attracted much attention due to their special characteristics, such as high photoluminescence (PL) quantum efficiencies,[3] tunable wavelength,[4–7] and large charge carrier diffusion length.[8] Red, green, and blue emitting PeLEDs have been reported,[9–18] and the green emitting PeLEDs with $CH_3NH_3PbBr_3$ ($MAPbBr_3$) have attracted more attention due to a recent reported PeLED with a current efficiency of 42.9 cd A^{-1}, opening up potential applications in display and lighting fields.[19]

A bright light emitted and high coverage perovskite film is a pre-requisite for high performance PeLEDs. However, due to the perovskite materials are easily crystal at low temperature, large grain size is easily formed during the perovskite film processing, resulting in poor coverage and large leakage current, thus poor device performance. Several methods have been carried out to improve the perovskite film quality and the PeLED performance. Numerous of interfacial layers and interfacial treatment methods have been introduced during the device processing, such as ultrathin polyethyleneimine modification layer,[12] amino acid modified ZnO,[20] ethanolamine modified TiO_2,[21] modified poly(3,4-ethylenedioxythiophene) doped with polystyrene sulfonic acid (PEDOT:PSS),[4] and electron transport layer $Zn_{1-x}Mg_xO$.[22] Moreover, blends of perovskite and polymers dielectric were reported to reduce pinholes and improve quantum efficiency.[23,24] Among all of these reported, film quality have been improved, but the device properties including luminance and current efficiency are relatively low, and need to be further improved.

As we know, during the perovskite film formation, two processes of spin-coating and annealing are the key for controlling the morphology of the perovskite film. Volatile solvent treatment is a popular method used in perovskite photovoltaic cells to induce fast crystallization of the perovskite material during spin-coating process.[25–27] In the last year, this method had been used by Cho *et al.* to control the grain size of perovskite film, which boosted the PeLED performance, revealing the highest current efficiency and external quantum efficiency so far.[19] More and more researchers have pay close attention to the spin-coating process during the PeLED fabrication. But comparing to a thin perovskite layer, it is difficult to control the morphology of a thick perovskite layer, resulting from the fast growth of the perovskite film in a slower solvent evaporation process during spin-coating from a highly concentrated solution. Therefore, it exhibits poor reproducibility in PeLED with a thick light emitting layer. Additionally, the overlooked annealing process is also very important for the perovskite crystals grow and film formation.

In this work, chlorobenzene (CB) was used as the solvent to induce fast crystallization and reduce the grain size during a thin $MAPbBr_3$ film formation. And the effect of annealing temperature and time on the perovskite films and devices have been investigated in detail. It is found that the annealing temperature and time have significantly impact on perovskite film and device

[a]*State Key Laboratory of Luminescence and Applications, Changchun Institute of Optics, Fine Mechanics and Physics, Chinese Academy of Sciences, Changchun 130033, China. E-mail: guoxy@ciomp.ac.cn; liuxy@ciomp.ac.cn*

[b]*University of Chinese Academy of Sciences, Beijing 100049, China*

† Electronic supplementary information (ESI) available. See DOI: 10.1039/c6ra14393h

properties. An anneal condition optimized PeLED shows a maximum luminance of 13 700 cd m^{-2}, and a maximum current efficiency of 8.22 cd A^{-1}. This work will provide useful information for the future optimization and development in high quality perovskite films and high performance PeLEDs.

Experimental

Fig. 1(a) shows the device configuration of the PeLED used in this study and the corresponding layers in the device have marked in the cross section scanning electron microscopy (SEM) image. All devices are constructed on the widely used transparent indium tin oxide (ITO) electrode, which was cleaned with acetone, alcohol, and deionized water in an ultrasonic bath and then baked at 120 °C for 30 min in an oven. After UV-ozone treated for 20 min, a 40 nm-thick PEDOT:PSS (Clevios P AI 4083) was spin coated on the ITO, and baked at 140 °C for 10 min on a hot plate. Subsequently, the samples were transferred into a N_2 glove box. A blend of CH_3NH_3Br (Xi'an Polymer Light Technology Corp., ≥99.5%) and $PbBr_2$ (Xi'an Polymer Light Technology Corp., >99.99%) in a 2 : 1 molar ratio (10 wt%) was spin-coated onto the samples from DMF for use as the active layer (4000 rpm, 30 s). During this spin-coating processing, 300 μl CB was dropped onto the sample at about 7th second. Then the samples were annealed at different temperatures on the hot plate. The thickness of the perovskite layer is about 60 nm. Finally, TPBi (30 nm), LiF (1 nm) and Al (100 nm) were thermally deposited in vacuum at a pressure of 3.0×10^{-4} Pa. The active area of the PeLED devices was 0.12 cm^2. All measurements were carried out in air without encapsulation.

Surface images of the composite films were obtained by SEM (Hitachi S-4800), and atomic force microscopy (AFM) measurements were performed with a Shimadzu SPA-9700. PL spectra were collected using a Shimadzu F-7000 spectrometer with an excitation wavelength of 360 nm and X-ray diffraction (XRD) patterns were carried out using a Bruker Advance D8 X-ray diffractometer. Photoluminescence quantum yields (PLQYs) of encapsulated films were obtained in a calibrated integrating sphere in FLS920 spectrometer. Ultraviolet-visible (UV-vis) absorption spectra were collected using a Shimadzu UV-3101PC spectrophotometer. The thickness of each film was measured using an Ambios XP-1 surface profiler. Current density *versus* voltage (*J*–*V*) and luminance *versus* voltage (*L*–*V*) characteristics were measured using a system incorporating a Konica-Minolta LS-110 Luminance Meter and a Keithley 2611 source-measure unit.

Results and discussion

Spin-coating and annealing are the two keys for controlling the morphology of the perovskite film in the device fabrication. Due to the high crystallinity, large $MAPbBr_3$ crystals are easily formed during spin-coating from DMF solution[14,15,23] as shown in Fig. 1(b). The large grain size (~200 nm) result in large non-radiative leakage current and large exciton diffusion length, thus poor PeLED performance. Solvent induced crystallization has been reported as an efficient method for morphology control in perovskite solar cells,[25,28,29] which has also been introduced in PeLEDs.[19,20] In this work, CB was used as the solvent to induce fast crystallization during the $MAPbBr_3$ film formation. Fig. 1(c) shows the SEM image of the $MAPbBr_3$ film treated with CB solvent. The grain size was reduced to about 50 nm after CB treatment.

In order to explore the effect of annealing temperature and time on the $MAPbBr_3$ film, a series of measurements were carried out. The luminescent properties of the films were

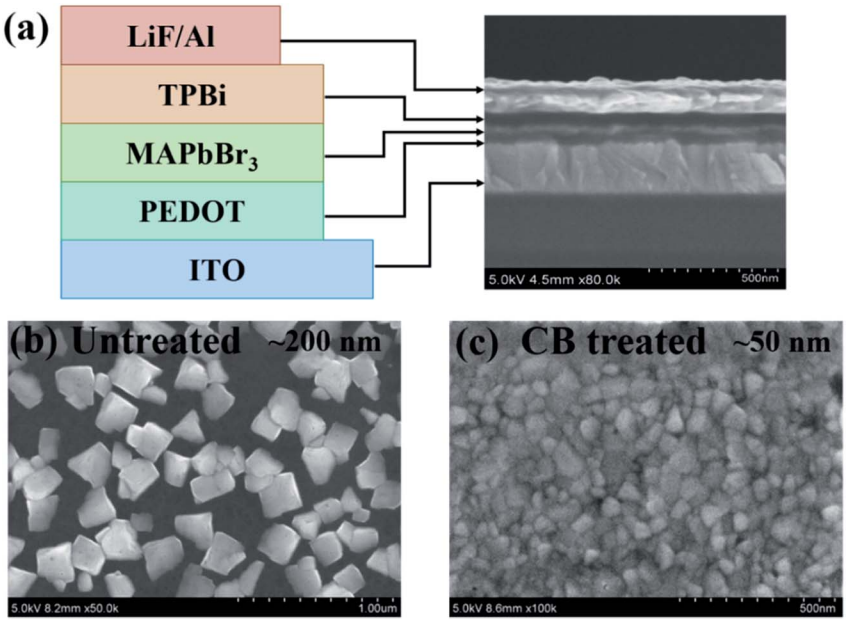

Fig. 1 (a) Device configuration and the cross section SEM of the PeLED used in this study. SEM images of the $MAPbBr_3$ films treated (b) without and (c) with CB solvent. Both of the films were annealed at 60 °C for 30 min.

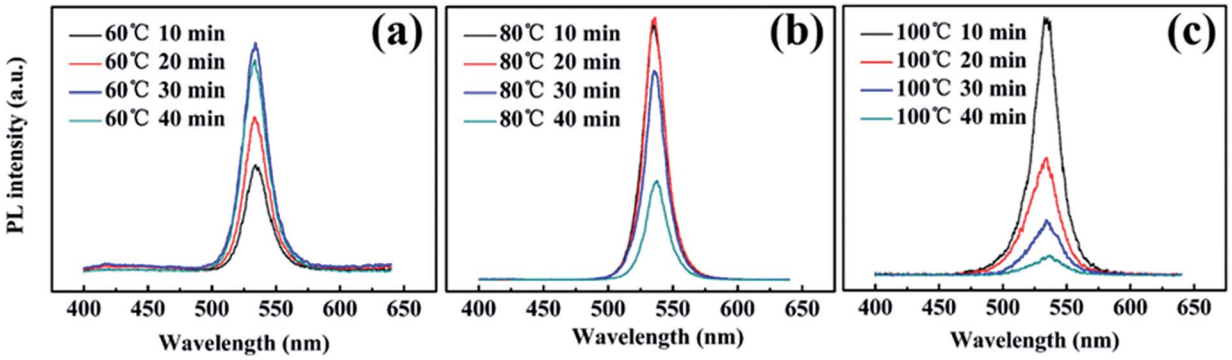

Fig. 2 PL spectra of $MAPbBr_3$ films annealed under (a) 60 °C, (b) 80 °C and (c) 100 °C.

studies by steady-state PL measurement. Fig. 2 shows the PL spectra of $MAPbBr_3$ films annealed under different temperatures (60 °C, 80 °C and 100 °C) for various time (10, 20, 30 and 40 min), and Table S1† shows the photophysical parameters of these films, including full width at half maximum (FWHM), absorption peak, maximum emission wavelength, and photoluminescence quantum yield (PLQY). The $MAPbBr_3$ film exhibits a PL peak around 530 nm. For the 60 °C and 80 °C annealed films (Fig. 2(a) and (b)), as the annealing time increasing, the PL intensity first climb up and then decline, the highest PL intensity were achieved in the film annealed for 30 min and 20 min, respectively. For the 100 °C annealed films, the highest PL intensity was achieved in the film annealed for 10 min, and then the PL intensity decreased significantly as further increasing the annealing time. The decreased PL intensity may be attributed to the increased defects in the $MAPbBr_3$ film which lead to increased charge trapping and non-radiative recombination (luminescence quenching).[30,31] However, from Fig. 2, it can be seen that a high PL can be achieved with annealing at low temperature (60 °C) for a long time or at high temperature (100 °C) for a short time. The PLQYs of the corresponding films (Table S1†) show similar variation tendency as PL spectra, and the maximum PLQY was achieved in the two films annealed at 80 °C for 10 min and 20 min.

Fig. 3 shows the XRD patterns of $MAPbBr_3$ films annealed under different temperatures (60 °C, 80 °C and 100 °C) for various time (10, 20, 30 and 40 min), which can reveal the crystal nature of the material under annealing processing. There can

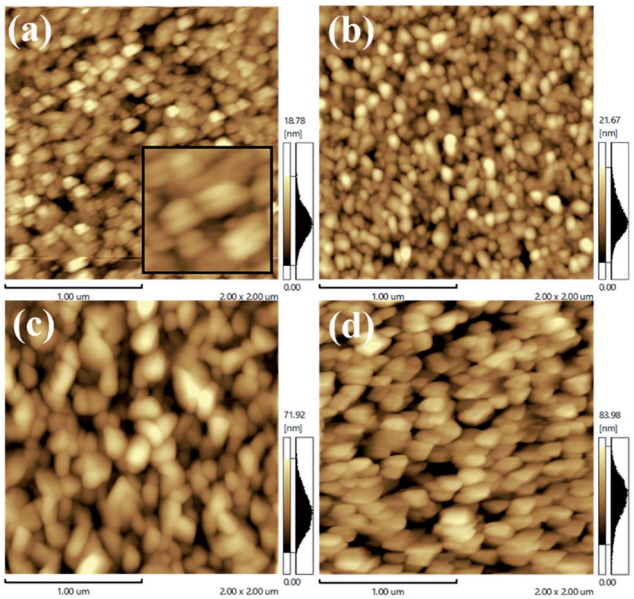

Fig. 4 AFM images of $MAPbBr_3$ films annealed under 100 °C for (a) 10 min, (b) 20 min, (c) 30 min and (d) 40 min. The enlarged image of (a) is shown in the inset of the figure.

be seen two sharp diffraction peaks at about 15.20° and 30.32° in the XRD patterns, which are assigned to (100) and (200) planes, respectively.[19,20] Among all of the samples, there is no $PbBr_2$ XRD pattern present,[32] suggesting complete conversion of

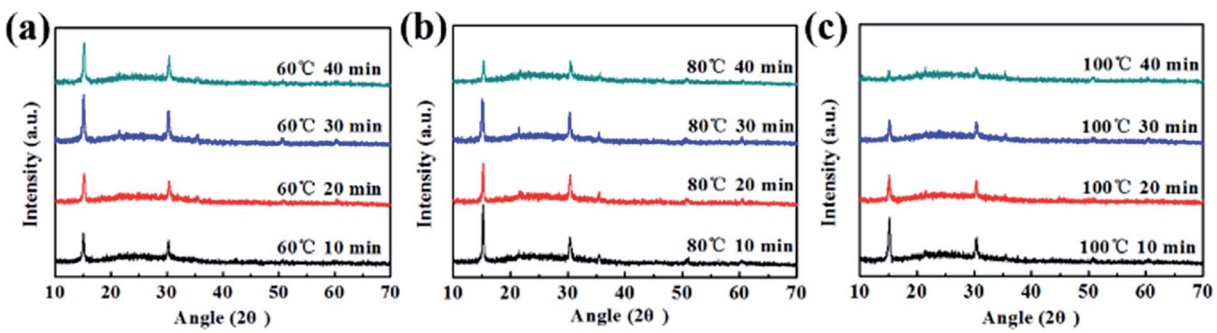

Fig. 3 XRD patterns of $MAPbBr_3$ films annealed under (a) 60 °C, (b) 80 °C and (c) 100 °C.

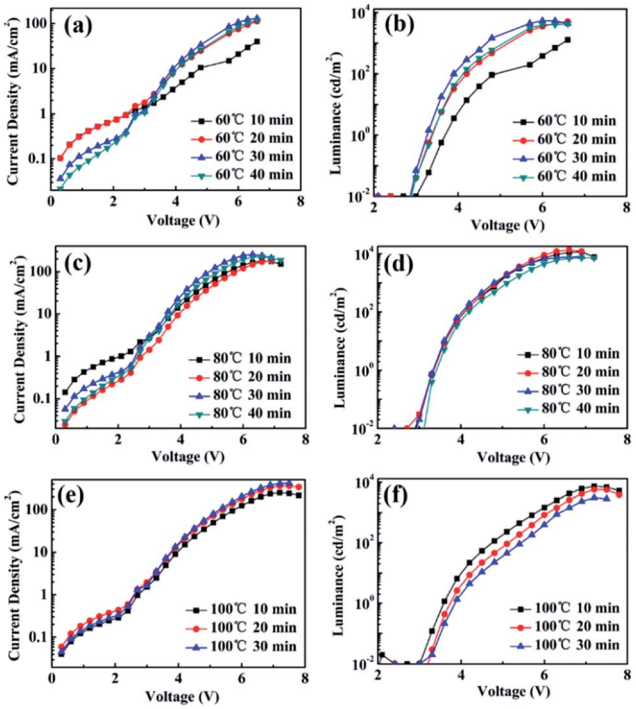

Fig. 5 *J–V* characteristics of PeLEDs annealed at (a) 60 °C, (c) 80 °C and (e) 100 °C. *L–V* characteristics of PeLEDs annealed at (b) 60 °C, (d) 80 °C and (f) 100 °C.

perovskite and absence of any degradation under different temperatures. For the 60 °C annealed films, the intensity of the XRD diffraction peaks for $MAPbBr_3$ was found to increase as the annealing time increasing, and reached higher value after annealing for 30 min. For the 80 °C annealed films, higher peak intensity can be found at the annealing time below 30 min, and the peak intensity decrease with annealing for 40 min. For the 100 °C annealed films, the peak intensity was found to decrease with the increased annealing time. Corresponding to the PL spectra shown in Fig. 2, the film with high XRD peak intensity was also found to exhibit high PL intensity, which indicates appropriate annealing temperature and time have positive effect on the $MAPbBr_3$ film formation.

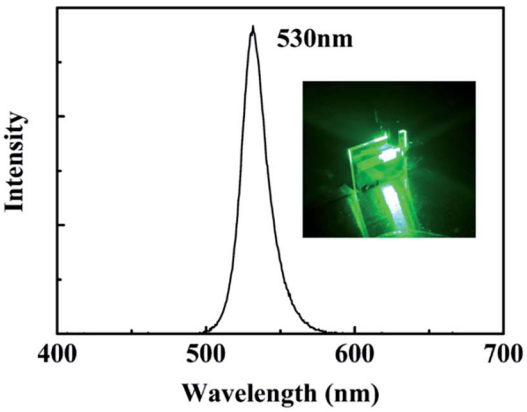

Fig. 6 EL spectrum of the PeLED with 80 °C annealed for 20 min. Photograph of this device is shown in the inset of the figure.

As seen in Fig. 2 and 3, the $MAPbBr_3$ films annealed at 100 °C show significant changes in PL and XRD spectra as the increased annealing time. So AFM measurement was carried out to establish relationship between the film morphology and PL or XRD characters and help us reveal the film growth process. Fig. 4 shows the AFM images of $MAPbBr_3$ films annealed under 100 °C for 10, 20, 30 and 40 min, respectively. It is seen in Fig. 4 that the grain size increases with the increased annealing time. The $MAPbBr_3$ crystals were small and dense at the first annealed 10 min and shown layer-by-layer growth which can be clearly seen in the enlarged image in Fig. 4(a). As the annealing time increased to 20 min, the crystals grown and fused to each other. When the annealing time increased to 30 min and 40 min, the grain size further increases. In order to understand the effect of the grain size on the film coverage, the coverage of the $MAPbBr_3$ films were calculated by using Image J software. The calculated coverage of the $MAPbBr_3$ films annealed under 100 °C for 10, 20, 30 and 40 min are 97.5%, 95.3%, 92.8% and 90.7%, respectively, which is found to decrease as the grain size increasing. The decreased coverage would result in increased pinholes in the $MAPbBr_3$ film, which also result in increased bulk trap states in the perovskite films with a high temperature annealed for a longer time.[31] Thus, as the annealing time increasing, decreased PL intensity was seen in Fig. 2(c). Therefore, proper annealing temperature and time

Table 1 Device parameters of PeLEDs annealed at different temperatures (60 °C, 80 °C and 100 °C) for various time (10, 20, 30 and 40 min)

Annealing temperature and time	Turn-on voltage (V)	Max. luminance (cd m^{-2})	Max. current efficiency (cd A^{-1})	Voltage for max. luminance (V)
60 °C 10 min	3.5 ± 0.2	1280 ± 500	3.21 ± 0.6	6.6 ± 0.2
60 °C 20 min	3.3 ± 0.2	5090 ± 1000	4.73 ± 0.6	6.6 ± 0.2
60 °C 30 min	3.2 ± 0.1	5370 ± 1500	5.07 ± 0.5	6.0 ± 0.4
60 °C 40 min	3.3 ± 0.1	4270 ± 1000	4.69 ± 0.6	6.6 ± 0.2
80 °C 10 min	3.2 ± 0.1	11 900 ± 2000	6.85 ± 0.7	6.9 ± 0.2
80 °C 20 min	3.2 ± 0.1	13 700 ± 2000	8.22 ± 0.8	6.6 ± 0.3
80 °C 30 min	3.2 ± 0.1	7980 ± 1500	3.81 ± 0.6	6.9 ± 0.2
80 °C 40 min	3.3 ± 0.2	7340 ± 1000	3.90 ± 0.6	6.9 ± 0.2
100 °C 10 min	3.3 ± 0.1	7330 ± 1500	2.93 ± 0.7	7.2 ± 0.3
100 °C 20 min	3.5 ± 0.2	5740 ± 1000	1.61 ± 0.6	7.2 ± 0.3
100 °C 30 min	3.6 ± 0.2	3070 ± 1000	0.75 ± 0.7	7.2 ± 0.3

are necessary for high luminance, good crystallinity and high coverage perovskite film.

The devices with the structure of ITO/PEDOT:PSS/$MAPbBr_3$/TPBi/LiF/Al (Fig. 1(a)) were fabricated. Fig. 5 shows the *J–V* and *L–V* properties of the PeLED annealed under different temperatures (60 °C, 80 °C and 100 °C) for various time (10, 20, 30 and 40 min). And Table 1 lists these device parameters, including turn-on voltage, maximum luminance, maximum current efficiency, and voltage for maximum luminance. For the 60 °C annealed devices, the current density of the PeLEDs with annealed over 30 min is smaller than that of the device with annealed 10, or 20 min at driven voltage below turn on voltage, indicating the suppression of leakage current by annealing for a longer time. The maximum current efficiency of 5.07 cd A^{-1} was achieved at the 30 min annealed device, with the highest luminance of 5370 cd m^{-2} at 6.0 V. For the 80 °C annealed devices, the current density of the PeLED with annealed for 20 min is smaller than those of the other devices at the same driven voltage, and the maximum current efficiency of 8.22 cd A^{-1} was also achieved at the 20 min annealed device, with the highest luminance of 13 700 cd m^{-2} at 6.6 V. For the 100 °C annealed devices, the maximum current efficiency of 2.93 cd A^{-1} was also achieved at the 10 min annealed device, with the highest luminance of 7980 cd m^{-2} at 7.2 V. The device performance degenerated significantly as the annealing time increasing, and the 40 min annealed device was hardly work (not shown in Fig. 5). The variation tendency of luminance in all of these devices is consistent with the PL spectra shown in Fig. 2. Among all of these PeLEDs, the devices with 80 °C annealed have better device performance than that of the devices with 60 °C or 100 °C annealed, and in the 80 °C annealed devices, 20 min annealed device has the best performance, indicating that the $MAPbBr_3$ film exhibited the best crystallinity and coverage. The EL spectrum of this device is shown in Fig. 6, which has an EL peak at 530 nm, consisted with its PL spectrum. And the bright device photograph is also shown in the inset of this figure.

Conclusions

In summary, the effect of annealing temperature and time on the perovskite films and devices have been investigated in detail. The properties including photoluminescence, crystallinity and morphology of perovskite films together with device performance have been affected significantly by the annealing temperature and time. It is found that an optimized annealing condition of the PeLED prepared in this work is 80 °C annealed for 20 min. The optimized device exhibits a maximum luminance of 13 700 cd m^{-2}, and a maximum current efficiency of 8.22 cd A^{-1}. We believe the annealing temperature and time studied in this work could be of great value for the further fabrication and development of high quality perovskite films and high performance PeLEDs.

Acknowledgements

This work is supported by the CAS Innovation Program, the National Natural Science Foundation of China No. 61106057, 6140031454 and 51503196, and the Jilin Province Science and Technology Research Project No. 20140520119JH, 20150101039JC, 20160520176JH and 20160520092JH, and project supported by State Key Laboratory of Luminescence and Applications.

Notes and references

1 N. J. Jeon, J. H. Noh, W. S. Yang, Y. C. Kim, S. Ryu, J. Seo and S. I. Seok, *Nature*, 2015, **517**, 476–480.
2 D. Bi, W. Tress, M. I. Dar, P. Gao, J. Luo, C. Renevier, K. Schenk, A. Abate, F. Giordano, J.-P. Correa Baena, J.-D. Decoppet, S. M. Zakeeruddin, M. K. Nazeeruddin, M. Gratzel and A. Hagfeldt, *Sci. Adv.*, 2016, **2**, e1501170.
3 F. Deschler, M. Price, S. Pathak, L. E. Klintberg, D. D. Jarausch, R. Higler, S. Huttner, T. Leijtens, S. D. Stranks, H. J. Snaith, M. Atature, R. T. Phillips and R. H. Friend, *J. Phys. Chem. Lett.*, 2014, **5**, 1421–1426.
4 Y. H. Kim, H. Cho, J. H. Heo, T. S. Kim, N. Myoung, C. L. Lee, S. H. Im and T. W. Lee, *Adv. Mater.*, 2015, **27**, 1248–1254.
5 G. Xing, N. Mathews, S. S. Lim, N. Yantara, X. Liu, D. Sabba, M. Gratzel, S. Mhaisalkar and T. C. Sum, *Nat. Mater.*, 2014, **13**, 476–480.
6 Z. Yuan, Y. Shu, Y. Xin and B. Ma, *Chem. Commun.*, 2016, **52**, 3887–3890.
7 Z. Yuan, Y. Shu, Y. Tian, Y. Xin and B. Ma, *Chem. Commun.*, 2015, **51**, 16385–16388.
8 Y. X. Zhai, C. X. Sheng, C. Zhang and Z. V. Vardeny, *Adv. Funct. Mater.*, 2016, **26**, 1617–1627.
9 Z. K. Tan, R. S. Moghaddam, M. L. Lai, P. Docampo, R. Higler, F. Deschler, M. Price, A. Sadhanala, L. M. Pazos, D. Credgington, F. Hanusch, T. Bein, H. J. Snaith and R. H. Friend, *Nat. Nanotechnol.*, 2014, **9**, 687–692.
10 L. Gil-Escrig, G. Longo, A. Pertegas, C. Roldan-Carmona, A. Soriano, M. Sessolo and H. J. Bolink, *Chem. Commun.*, 2015, **51**, 569–571.
11 A. Sadhanala, S. Ahmad, B. Zhao, N. Giesbrecht, P. M. Pearce, F. Deschler, R. L. Z. Hoye, K. C. Goedel, T. Bein, P. Docampo, S. E. Dutton, M. F. L. De Volder and R. H. Friend, *Nano Lett.*, 2015, **15**, 6095–6101.
12 J. Wang, N. Wang, Y. Jin, J. Si, Z. K. Tan, H. Du, L. Cheng, X. Dai, S. Bai, H. He, Z. Ye, M. L. Lai, R. H. Friend and W. Huang, *Adv. Mater.*, 2015, **27**, 2311–2316.
13 S. G. Bade, J. Li, X. Shan, Y. Ling, Y. Tian, T. Dilbeck, T. Besara, T. Geske, H. Gao, B. Ma, K. Hanson, T. Siegrist, C. Xu and Z. Yu, *ACS Nano*, 2016, **10**, 1795–1801.
14 B. Jiao, X. Zhu, W. Wu, H. Dong, B. Xia, J. Xi, T. Lei, X. Hou and Z. Wu, *Nanoscale*, 2016, **8**, 11084–11090.
15 J. C. Yu, B. Kim da, E. D. Jung, B. R. Lee and M. H. Song, *Nanoscale*, 2016, **8**, 7036–7042.
16 X. Zhang, H. Lin, H. Huang, C. Reckmeier, Y. Zhang, W. C. Choy and A. L. Rogach, *Nano Lett.*, 2016, **16**, 1415–1420.
17 J. C. Yu, D. W. Kim, D. B. Kim, E. D. Jung, J. H. Park, A. Y. Lee, B. R. Lee, D. Di Nuzzo, R. H. Friend and M. H. Song, *Adv. Mater.*, 2016, DOI: 10.1002/adma.201601105.
18 Y. Ling, Z. Yuan, Y. Tian, X. Wang, J. C. Wang, Y. Xin, K. Hanson, B. Ma and H. Gao, *Adv. Mater.*, 2016, **28**, 305–311.

19 H. C. Cho, S. H. Jeong, M. H. Park, Y. H. Kim, C. Wolf, C. L. Lee, J. H. Heo, A. Sadhanala, N. Myoung, S. Yoo, S. H. Im, R. H. Friend and T. W. Lee, *Science*, 2015, **350**, 1222–1225.
20 N. Wang, L. Cheng, J. Si, X. Liang, Y. Jin, J. Wang and W. Huang, *Appl. Phys. Lett.*, 2016, **108**, 141102.
21 J. C. Yu, B. Kim da, G. Baek, B. R. Lee, E. D. Jung, S. Lee, J. H. Chu, D. K. Lee, K. J. Choi, S. Cho and M. H. Song, *Adv. Mater.*, 2015, **27**, 3492–3500.
22 R. L. Hoye, M. R. Chua, K. P. Musselman, G. Li, M. L. Lai, Z. K. Tan, N. C. Greenham, J. L. MacManus-Driscoll, R. H. Friend and D. Credgington, *Adv. Mater.*, 2015, **27**, 1414–1419.
23 G. Li, Z. K. Tan, D. Di, M. L. Lai, L. Jiang, J. H. Lim, R. H. Friend and N. C. Greenham, *Nano Lett.*, 2015, **15**, 2640–2644.
24 J. Li, S. G. Bade, X. Shan and Z. Yu, *Adv. Mater.*, 2015, **27**, 5196–5202.
25 J. W. Jung, S. T. Williams and A. K. Y. Jen, *RSC Adv.*, 2014, **4**, 62971–62977.
26 J. W. Jung, C.-C. Chueh and A. K. Y. Jen, *Adv. Mater.*, 2015, **27**, 7874–7880.
27 N. J. Jeon, J. H. Noh, Y. C. Kim, W. S. Yang, S. Ryu and S. I. Seok, *Nat. Mater.*, 2014, **13**, 897–903.
28 K. Kara, D. A. Kara, C. Kirbiyik, M. Ersoz, O. Usluer, A. L. Briseno and M. Kus, *RSC Adv.*, 2016, **6**, 26606–26611.
29 K. F. Lin, S. H. Chang, K. H. Wang, H. M. Cheng, K. Y. Chiu, K. M. Lee, S. H. Chen and C. G. Wu, *Sol. Energy Mater. Sol. Cells*, 2015, **141**, 309–314.
30 M. Saba, M. Cadelano, D. Marongiu, F. Chen, V. Sarritzu, N. Sestu, C. Figus, M. Aresti, R. Piras, A. G. Lehmann, C. Cannas, A. Musinu, F. Quochi, A. Mura and G. Bongiovanni, *Nat. Commun.*, 2014, **5**, 5049.
31 W. Peng, B. Anand, L. Liu, S. Sampat, B. E. Bearden, A. V. Malko and Y. J. Chabal, *Nanoscale*, 2016, **8**, 1627–1634.
32 X. Fang, K. Zhang, Y. Li, L. Yao, Y. Zhang, Y. Wang, W. Zhai, L. Tao, H. Du and G. Ran, *Appl. Phys. Lett.*, 2016, **108**, 071109.